Meteorol. Appl. 10, 197–209 (2003) DOI:10.1017/S1350482703002081

A case study of tropopause cyclogenesis

Aarnout van Delden & Roel Neggers, *Institute for Marine and Atmospheric Sciences, Utrecht University, Princetonplein 5, 3584 CC Utrecht, The Netherlands*
e-mail: a.j.vandelden@phys.uu.nl

This paper is concerned with the transformation of an upper level trough into a shear line and a tropopause cyclone or cut-off low. During this event, the isentropic potential vorticity of air columns between fixed isentropes approaching the trough axis at its level of maximum intensity from the west is well conserved over a period of about 12 to 24 hours, but there is a significant repartitioning of the constituent parts, from a relatively large static stability to a relatively large absolute vorticity. This indicates stretching of vertical columns of air. The effect that is inducing the vortex stretching is identified within the context of quasi-geostrophic theory as 'opposite vector-frontogenesis'. This implies that Q-vectors point in opposite directions, respectively, above and below the level of maximum trough-intensity. Isentropic analysis indicates that the criterion for unstable isentropic downgliding is fulfilled in the upper troposphere in a restricted area, covering several hundred thousand square kilometres, near the base of the trough when and where the cut-off low is formed. This area of unstable isentropic downgliding, to which we assign the term 'baroclinic downburst', and which maintains its identity during a period of time in the order of 24 hours, coincides approximately with the dry intrusion as identified on a 'water vapour' image. It is argued that unstable isentropic downgliding is in fact necessary in order to realise a cyclone-core characterised by relatively high static stability, relatively high absolute vorticity and relatively high potential vorticity, as is demanded by the invertibility principle for potential vorticity. The events described above are triggered by the interaction of two potential vorticity anomalies.

1. Introduction

Weather systems which form and remain confined to the region near the tropopause are of interest not only to synopticians but also to atmospheric chemists, who want to know more about the exchange of, for example, ozone between the troposphere and the stratosphere. An example of such a weather system is the so-called 'cut-off low' or 'tropopause cyclone', being a closed cyclonic circulation in the upper troposphere and lower stratosphere. This paper is concerned with the dynamics of the atmosphere preceding and during the formation of a tropopause cyclone.

In middle latitudes tropopause cyclones are the result of a dynamical process in which a mass of air with high potential vorticity is 'cut off' from the polar stratosphere and becomes isolated in the mid-latitude troposphere (see e.g. Hoskins 1997). Kleinschmidt (1950a, 1950b), Eliassen & Kleinschmidt (1957) and Thorpe (1985) have shown that an isolated air mass of relatively high potential vorticity at upper levels, in geostrophic and hydrostatic equilibrium, is associated with a cyclonic circulation with depressed isentropic surfaces above and raised isentropic surfaces below, which is in accord with the observed structure of a cut-off cyclone (Palmen & Newton 1969), i.e. a pool of air with high potential temperature is found above the circulation centre while a pool of air with low potential temperature is found below the circulation centre. In the circulation centre one finds anomalously high values of both absolute vorticity *and* static stability. Thus, it seems that we have a relatively complete theory of the formation of cut-off cyclones. However, this theory does not give much insight into the actual dynamics of the cyclogenesis, in terms of air flow, absolute vorticity changes, divergence, vertical motion and associated changes in temperature.

The synoptic processes accompanying tropopause cyclogenesis have been investigated by several authors. Palmen (1949) was perhaps the first to describe in some detail the development of a cut-off low. He identified the strong upper tropospheric convergence connected with the subsidence and the associated vortex stretching leading to an increase in the relative vorticity. Hsieh (1949) stressed the importance of cross-stream vertical circulations in producing a cold dome in the lower troposphere and a lowering of the tropopause. Bell & Keyser (1993) investigated the significant interchanges between shear and curvature potential vorticity, resulting in the detachment of the potential vorticity anomaly from the 'stratospheric reservoir'. Bell & Bosart (1993) showed that cut-off cyclone formation follows

the descent of stratospheric air in a northwesterly flow to lower levels in conjunction with the propagation of a pre-existing intensifying jet streak toward the base of a long wave diffluent trough.

Hsieh (1950) investigated a phenomenon which is closely related to the cut-off cyclone, namely the 'upper shear line'. A shear line is an elongated, relatively narrow zone across which there is a clear change in the horizontal wind direction, and which is therefore a zone of high absolute value of the vorticity. Shear lines are observed frequently in the upper troposphere and the lower stratosphere and especially near the level of the tropopause. They are also visible at these levels as streamers or filaments of high potential vorticity (e.g. Appenzeller *et al*. 1996). Shear lines at the tropopause are usually associated with intrusions of stratospheric air into the troposphere. Many cut-off cyclones form from a trough which has been transformed into an upper shear line, i.e. a trough with a very small width and large meridional amplitude. The upper shear line was also investigated by Newton *et al*. (1951) and Holopainen & Rontu (1981). These studies elucidated the important role played by cross-stream vertical circulations and vortex stretching in shear line formation. Nevertheless, Holopainen & Rontu (1981), who pay attention only to shear line dissipation and not to shear line formation, state that 'it has become clear that the basic elements of shear line formation are already included in the dynamics of two-dimensional non-divergent flow'. This is supported by numerical simulations performed by, for example, Polvani & Plumb (1992). However, it is frequently observed that shear line and cut-off low formation is accompanied by a spectacular and relatively sudden increase of the absolute vorticity, which is a three-dimensional effect. This paper therefore focuses on the three-dimensional aspects of the flow and the temperature associated with shear line and cut-off low formation.

Thorncroft *et al*. (1993) found by numerical simulation that the typical shear line is the end-product in the upper troposphere of one of two possible life cycles of a baroclinic wave. This particular kind of life cycle was termed 'LC1'. According to Thorncroft *et al*. (1993), on the nineth day of LC1 the upper level shear line is located over an area with an anticyclone at the earth's surface. The present paper is concerned with this kind of development.

According to Hirschberg & Fritsch (1991a, 1991b), who investigated the temperature evolution during upper-level trough amplification, trough development is accompanied by a lower-stratospheric temperature increase and mid-tropospheric temperature decrease within the trough region. We think that the vertical motion associated with thermal wind adjustment to the changing peculiar pattern of isentropes in the region around the tropopause is an important aspect of the dynamics of upper tropospheric cyclogenesis.

The structure of the paper is as follows. First (in section 2) we will describe the general synoptic situation in a particular case of cut-off low formation. Using this case we present and verify a conceptual Lagrangian view of the dynamics of air columns entering the base of a trough (section 3). These air columns undergo vortex stretching as they approach the trough base from the west. In section 4 we show that the vertical motion associated with this vortex stretching is associated with the adjustment to the horizontal distortion of isentropes near the axis of the trough. In section 5 we uncover events at higher levels in the atmosphere that appear to influence the formation of the cut-off low around the tropopause. In section 6 we estimate the importance of non-adiabatic effects and discover that the cut-off low forms in a region of several hundred thousand square kilometres where the motion can be characterised as 'unstable isentropic downgliding'. The paper is concluded in section 7 with a short overview and discussion of the results.

2. Typical synoptic situation preceding upper level cyclogenesis

We use analyses of wind, temperature and geopotential on a regular grid in the horizontal plane and on 11 standard pressure levels made at the European Centre for Medium-Range Weather Forecasts (ECMWF). The distance between gridpoints is 1° in both the zonal and meridional direction. The time interval between analyses is 6 hours. The datasets on isentropes are obtained by interpolation between pressure surfaces (see Eduard *et al*. 1997). The static stability is calculated for a layer between isentropes with a thickness of 10 K. Partial derivatives with respect to x, y and p are approximated by centred finite differences.

The event chosen occurred between 8 May and 10 May 1996 in north-west Europe. Figure 1 shows the analysis of isentropic absolute vorticity on the 310K isentropic surface. This isentrope is a so-called middle-world isentrope (Hoskins 1991), i.e. it intersects the tropopause, which is defined as the 2 PVU iso-potential vorticity surface. On 9 May 1996, 0000 UTC (Figure 1a) a trough can be observed in the upper troposphere, lying over the North Sea. High windspeeds are found in the north-westerly flow upstream and in the south-westerly flow downstream of the base of the trough. Between 0000 UTC and 1200 UTC, 9 May 1996, the trough contracts in an east-west direction, forming a shear line (Figure 1b), or an elongated band of high isentropic potential vorticity, frequently termed a 'streamer' (e.g. Appenzeller *et al*. 1996; Cox *et al*. 1997). The absolute vorticity in the centre of the shear line increases significantly (Figure 1a and 1b). The elongation of the shear line continues on 10 May (Figure 1c and 1d) until the vorticity maximum at the base of the trough is cut off. The sudden increase of the vorticity during a 12-hour period prior to the

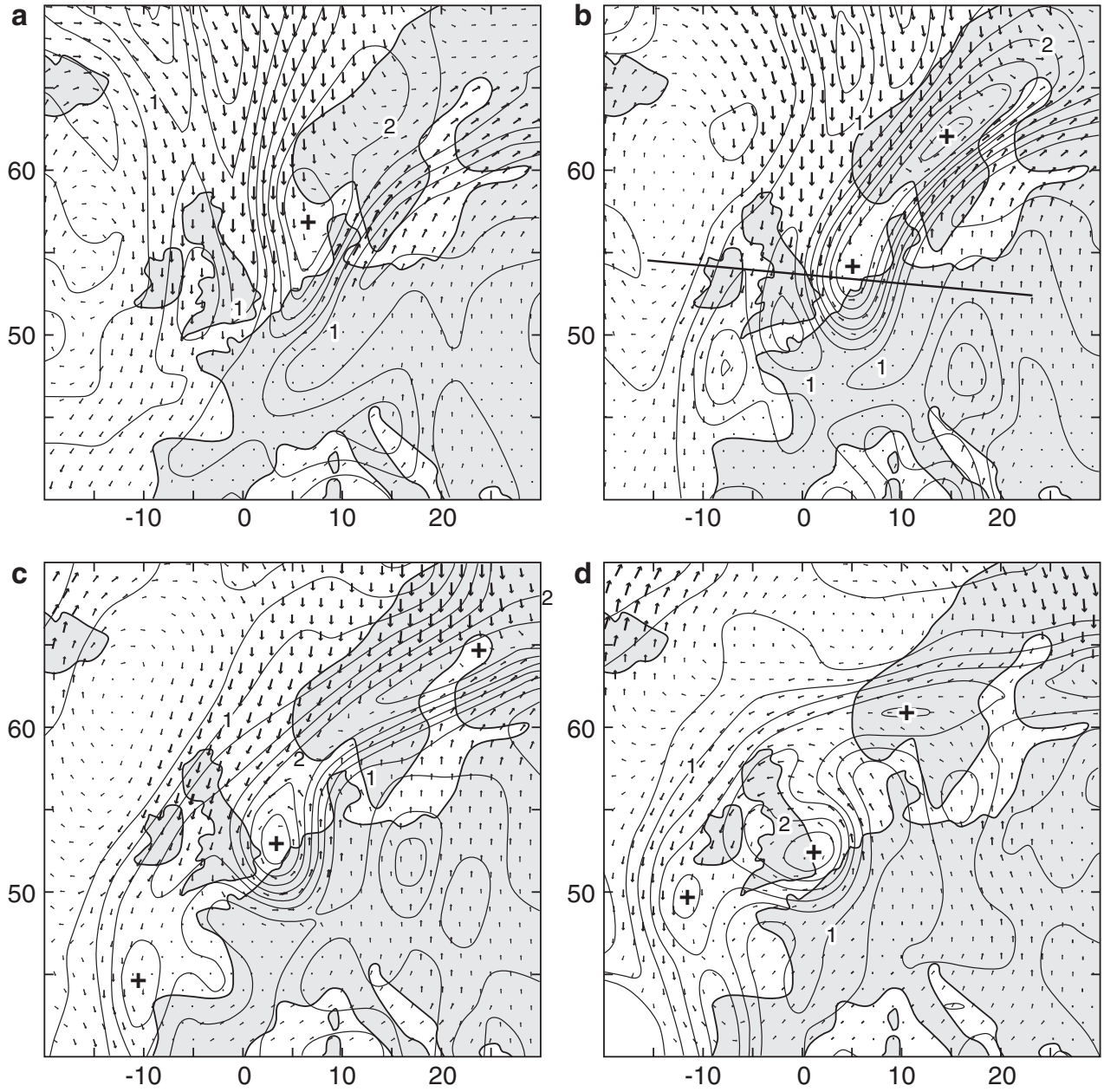

Figure 1. *The absolute vorticity (labeled in units 10^{-4} s^{-1}) on the 310 K isentrope (at about 6 to 8 km above sea level) and the associated windfield corresponding to (a) 9 May 1996, 00 UTC; (b) 9 May 1996, 12 UTC; (c) 10 May 1996, 00 UTC; and (d) 10 May 1996, 12 UTC. The horizontal axis is the longitude east of Greenwich, the vertical axis is the latitude. Note the strong increase of the absolute vorticity on 9 May, and the collapse of the shear line on 10 May.*

appearance of the cut-off low is an event which demands an explanation.

Figure 2 shows the six-hour isobaric height change and temperature change (prior to 9 May, 12 UTC) in a vertical cross-section along the line indicated in Figure 1b. We see that cyclogenesis (negative isobaric height change) is associated with positive temperature tendencies in the lowest 3 km of the stratosphere and negative temperature tendencies in the upper half of the troposphere. There is very little happening near the earth's surface as far as isobaric height changes are concerned.

The trough, the shear line and, later, the cut-off cyclone can also be recognised clearly in the analysis of the isentropic potential vorticity (PV) (Figure 3). A qualitative inspection of Figure 3 suggests that the PV within the trough is materially conserved, implying that conditions at this level in the atmosphere are adiabatic. Because the mass and the PV of air columns is conserved, the collapse of the trough into a relatively thin filament or streamer of PV must necessarily be accompanied by vortex stretching. Our intention in this paper is to identify a mechanism that causes the stretching and the accompanying increase of the absolute vorticity.

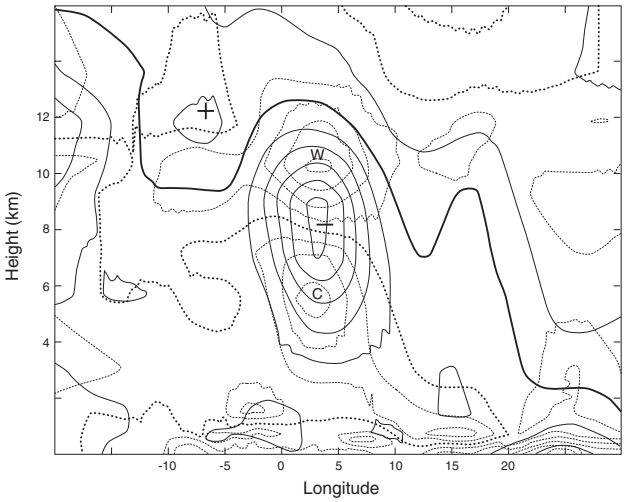

Figure 2. *Vertical section along the line indicated in Figure 1b showing the isobaric height- and temperature-changes during the 6 hours prior to 9 May 1996, 12 UTC. Contour-intervals are 10 m for height changes (solid lines) and 1 K for temperature changes (stippled lines). The thicker lines correspond to the zero-isopleth.*

3. Vortex stretching

Our hypothetical conceptual model of trough intensification is illustrated in Figure 4. Stably stratified air with relatively high potential vorticity is advected into the base of the trough, and is subject to vertical stretching, forced by vertical motions of opposite sign induced by a mechanism which we will identify as 'opposite vector-frontogenesis' in the next section.

To demonstrate that these events are actually taking place in this case, the movement of columns of air between middle world isentropes is investigated, and an analysis is made of the relationship between isentropic potential vorticity, static stability and absolute vorticity of the columns. The isentropic potential vorticity, Z_θ, is defined as

$$Z_\theta = -g(\zeta_\theta + f)\frac{\partial \theta}{\partial p} \qquad (1)$$

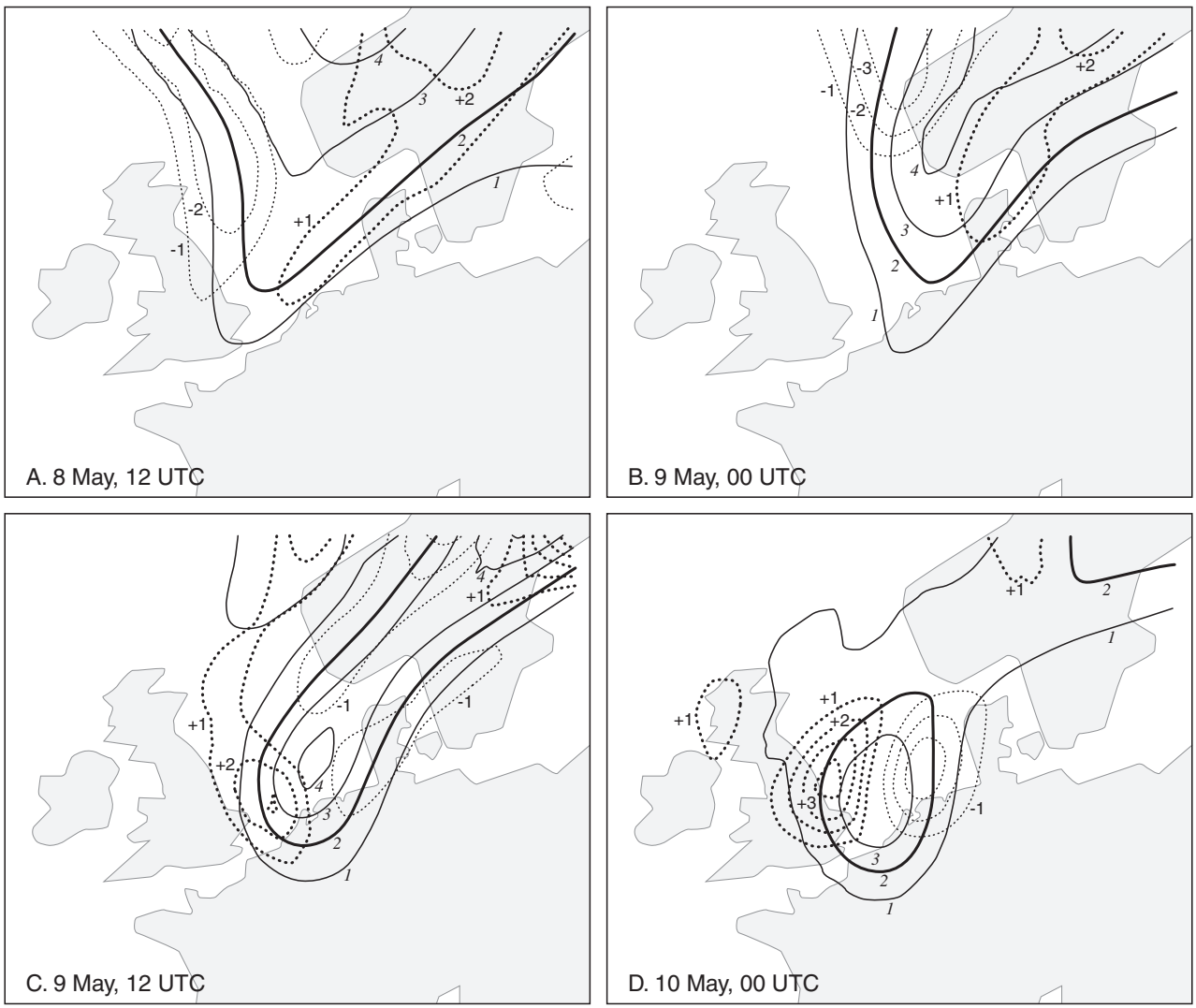

Figure 3. *Distribution of the isentropic potential vorticity (solid lines; labels in PVU; 1 PVU is 10^{-6} K m^{2}Kg^{-1}s^{-1}) and of the advection of potential vorticity (stippled lines; labels in units of 0.1 PVU hr^{-1}) within the layer 305–315 K over western Europe on 8 May, 12 UTC (A); 9 May, 00 UTC (B); 9 May, 12 UTC (C); and 10 May, 00 UTC (D). The changes in the advection of potential vorticity are discussed in section 5.*

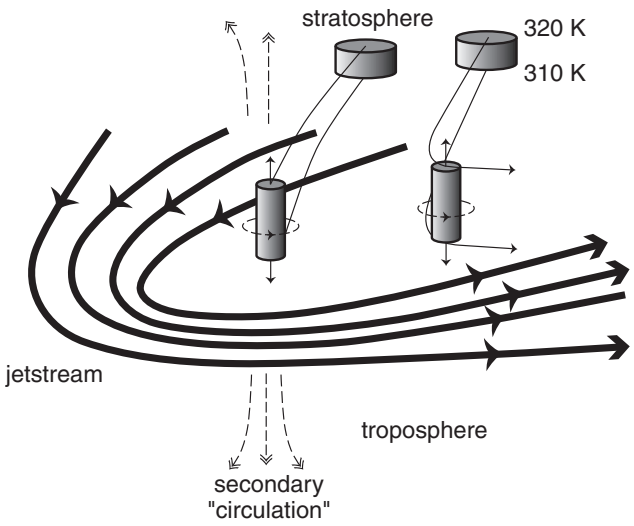

Figure 4. *A schematic picture of the events leading to the formation of a shear line due to vortex stretching forced by frontogenesis of opposite sign, respectively, above and below the tropopause*

where ζ_θ is the relative vorticity at constant potential temperature (θ), f is the Coriolis parameter, g is the acceleration due to gravity and p is the pressure.

The isentropic layer between 310 K and 320 K is chosen for study, because at the height of these isentropes (approximately 6 to 9 km) the strongest changes in absolute vorticity are observed. Within the region of interest, the 320 K isentrope slopes upwards towards the south, while the 310 K isentrope slopes downwards towards the south.

The movement of a column of air between 310 K and 320 K can be approximated by calculating the path of an air parcel at the top (320K), middle (315K) and bottom (310K). Suppose that an air parcel at time $t=n\Delta t$ (where n is a positive integer and Δt is a time interval), has a velocity $\vec{v}$ and a position $\vec{x}$, then

$$\frac{\mathrm{d}\vec{x}}{\mathrm{d}t} = \vec{v}(\vec{x},t). \qquad (2)$$

The new position $\vec{x}^*$ of the air-particle at $t=(n+1)\Delta t$ can be estimated by:

$$\vec{x}^*(n+1) = \vec{x}(n) + \Delta t\vec{v}(n). \qquad (3)$$

A second estimate can be calculated from $\vec{v}$ (n) and $\vec{v}^*$ (n+1) by:

$$\vec{x}(n+1) = \vec{x}(n) + \Delta t\left(\alpha\vec{v}(n) + \beta\vec{v}^*(n+1)\right) \qquad (4)$$

Repeating this with α=1/2 and β=1/2 (this actually is the Heun-scheme, see Mesinger & Arakawa 1976) and Δt=60 s gives a satisfactory result. The velocity $\vec{v}$ at position $\vec{x}$ is calculated by linear interpolation in time and space between the adjacent gridpoints.

Because of the different windfields on the three isentropic surfaces, the trajectories of the air parcels on those isentropes may differ significantly. This means that columns of air are stretched not only vertically but also horizontally, i.e. the axis of the column is tilted to the vertical. If only the vertical stretching is accounted for, this may cause a deviation of the calculated stretching from the real stretching. Figure 5 shows four examples. In three examples, the three trajectories stay reasonably close together for a period of 18 hours. However, in the other example (Figure 5c) the trajectories on the different isentropes differ significantly.

The consequences of this problem for determining the conservation of isentropic potential vorticity can be seen in Figure 6, which shows a scatter plot of the static stability ($\equiv -\partial\theta/\partial p$) against the mean isentropic absolute vorticity in the column for the four cases shown in Figure 5. In the case of weak tilting (cases a, b and d in Figure 5), the points show a highly significant correlation to the hyperbolic regression curve, with correlation coefficients of 0.97 and 0.98. This proves that the stretching of a column of air (i.e. the decrease of the static stability) results in an increase in absolute vorticity in the column, in accordance with the law of conservation of isentropic potential vorticity for adiabatic flow.

The evolution in time of isentropic potential vorticity, of static stability and of absolute vorticity of one particular column of air (case d in Figure 5) is shown in Figure 7. It nicely illustrates that, while the air column is advected towards the axis of the trough, between 00 UTC and 12 UTC on 9 May the static stability decreases and the absolute vorticity increases, while the potential vorticity remains approximately constant. The value of Z_θ for this particular column of air fluctuates by only about 1% around the mean value of nearly 4 PVU, while the changes in static stability and absolute vorticity during the same period are of the order of 30 %.

4. Frontogenesis-vector

Inspired by the work of Hoskins *et al.* (1978), Keyser *et al.* (1988) and Kurz (1997), we now investigate the role of frontogenesis in the vortex stretching demonstrated in the previous section. The frontogenesis-vector is defined as the temporal rate of change along an air parcel trajectory of the horizontal temperature gradient, i.e. as

$$\frac{\mathrm{d}\vec{\nabla}_\mathrm{h}T}{\mathrm{d}t} \equiv \frac{\mathrm{d}}{\mathrm{d}t}\left(\frac{\partial T}{\partial x}, \frac{\partial T}{\partial y}\right), \qquad (5)$$

where x and y are, respectively, the zonal and the meridional coordinate and T is the temperature. Within the context of quasi-geostrophic theory, we can write (Holton 1992)

$$\frac{\mathrm{d}_\mathrm{g}\vec{\nabla}_\mathrm{h}T}{\mathrm{d}t} \equiv \vec{Q} = \left(\frac{\partial\vec{v}_\mathrm{g}}{\partial x}\cdot\vec{\nabla}T, \frac{\partial\vec{v}_\mathrm{g}}{\partial y}\cdot\vec{\nabla}T\right), \qquad (6)$$

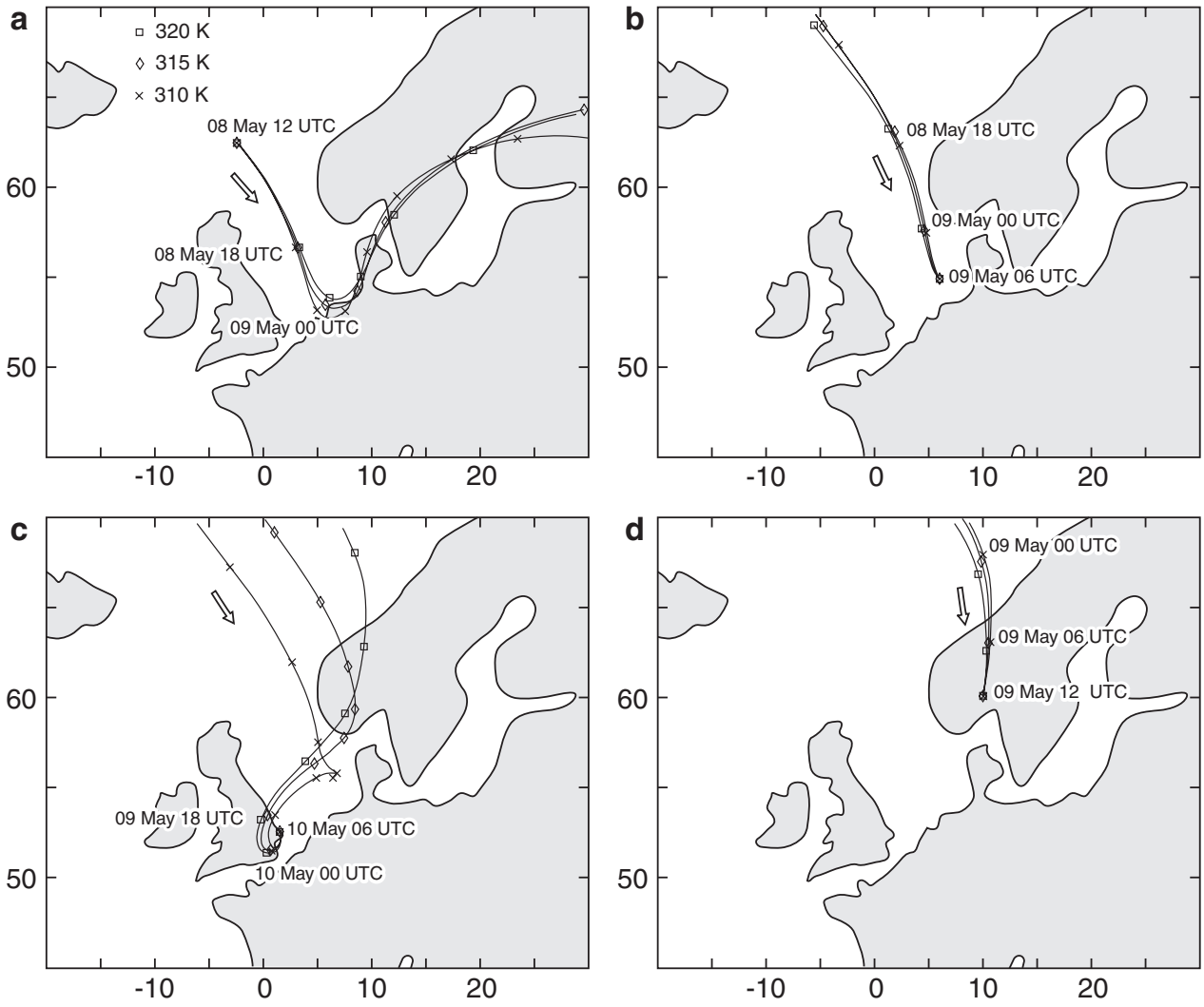

Figure 5. *Trajectories of air parcels on, respectively, the 310 K isentrope (position at 6-hour intervals marked by a cross), the 315 K isentrope and the 320 K isentrope (position at 6-hour intervals marked by a square). These parcels form a 'column' of air, which, in adiabatic conditions, remains between the 310 K isentrope and the 320 K isentrope. Columns b, c and d travel towards a fixed point on the axis of the trough. The arrow marks the direction of movement along the trajectories.*

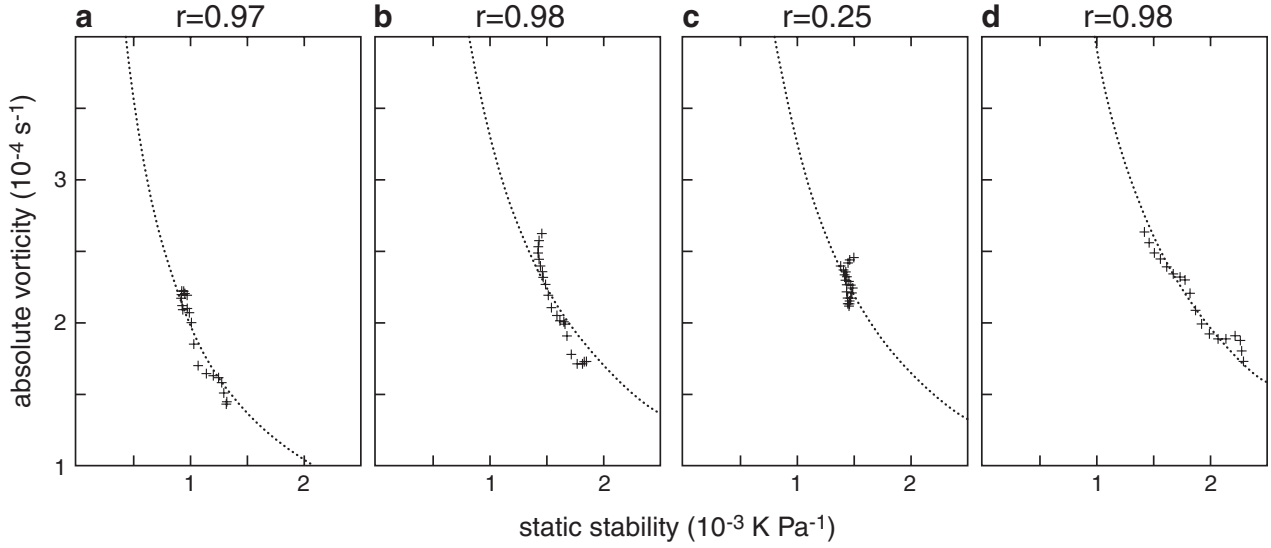

Figure 6. *The static stability and absolute vorticity of the 'columns' of air for which the trajectories are displayed in Figure 5. Each cross marks a time point in the trajectory. The dotted line is the least square fit to the hyperbole y=A/x. The parameter, r, is the correlation coefficient of the points compared to this hyperbole. Figure 6 (a, b, c and d) correspond to Figure 5 (a, b, c and d), respectively.*

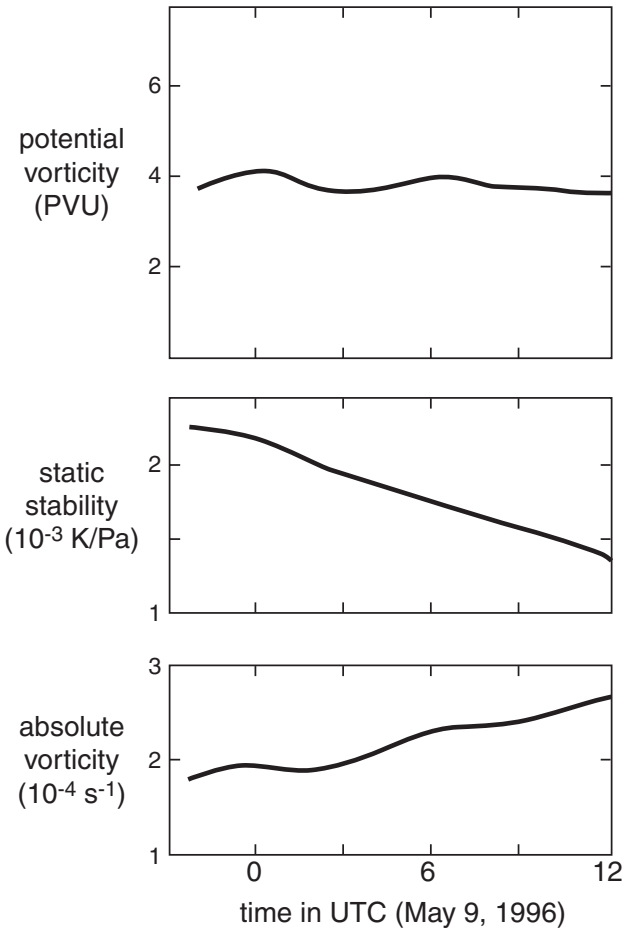

Figure 7. *Isentropic potential vorticity, static stability and absolute vorticity of the air column whose trajectory is shown in Figure 5d.*

where $d_g/dt = \partial/\partial t + \vec{v}_g \cdot \vec{\nabla}_p$, with $\vec{v}_g \equiv (u_g, v_g)$ the geostrophic wind-vector. All derivatives with respect to x and y are taken with pressure held constant.

In a relatively sharp symmetric trough with an axis oriented in the meridional direction (along the y-axis), embedded in a temperature field with a gradient oriented parallel to the axis of the trough, the Q-vector can be approximated by

$$\vec{Q} \approx \left(-\frac{\partial v_g}{\partial x}\frac{\partial T}{\partial y}, 0 \right) \approx \left(-\zeta_g \frac{\partial T}{\partial y}, 0 \right), \qquad (7)$$

where ζ_g is the geostrophic relative vorticity. The approximation, $\zeta_g \approx \partial v_g/\partial x$, is valid if $\partial u_g/\partial y << \partial v_g/\partial x$. Since $\zeta_g > 0$ and below the level of maximum wind speed we have $\partial T/\partial y < 0$, the Q-vector at the trough axis points in easterly direction. However, above the level of maximum wind speed we have $\partial T/\partial y > 0$, which implies that the Q-vector points in westerly direction. The important thing to note here is that the frontogenesis-vector below and above the jetstream core, respectively, points in opposite directions.

Both the rotation of the isobaric temperature gradient as well as the intensification and weakening of the isobaric temperature gradient have the effect of disrupting thermal wind. In order to preserve thermal wind balance, ageostrophic motion is required. The sign of the vertical component of this motion can be deduced from the divergence of the Q-vector (Hoskins *et al.* 1978). It appears that Q-vector divergence (convergence) is associated with downward (upward) motion. Based on (7), we thus expect downward motion to the west of the trough below the level of maximum wind speed. However, above this level (in the stratosphere) we expect upward motion to the west of the trough.

Figure 8, which shows the time average Q-vector divergence at, respectively, 250 hPa (upper panel) and

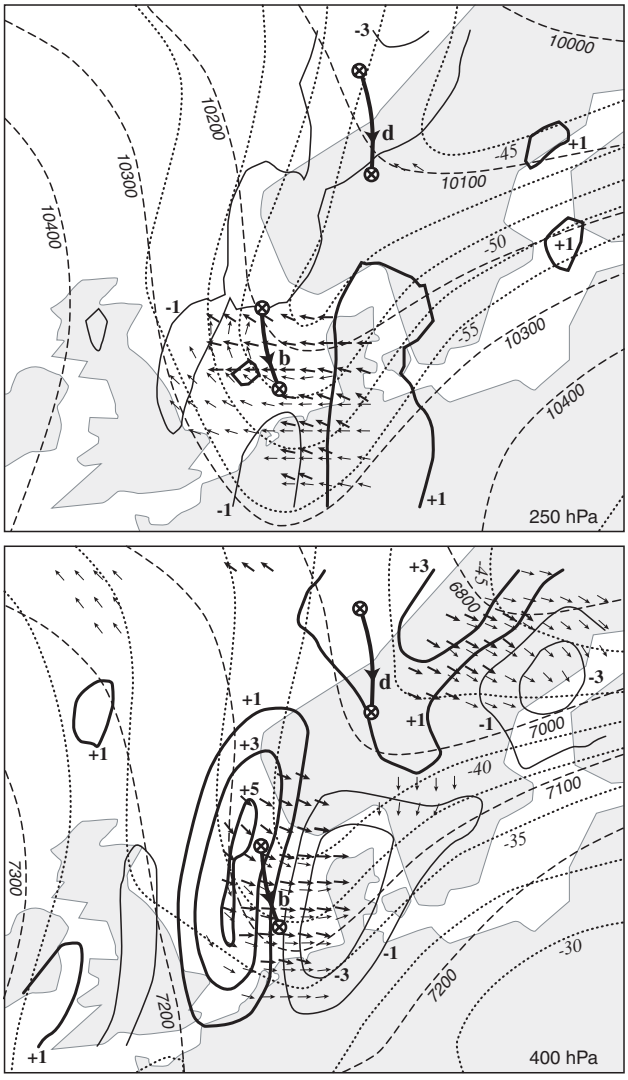

Figure 8. *Q-vectors at two points in time (thick arrows correspond to 9 May, 00 UTC; thin arrows correspond to 9 May, 06 UTC) (only shown if $|\vec{Q}| > 5\times10^{-10}$ K m^{-1} s^{-1}), Only the direction $\vec{Q}$ is shown, not the magnitude. Also shown are isopleths of the time average isobaric height (dashed lines) (labeled in m), the time average temperature (stippled lines) (labeled in °C) and the time average divergence of the Q-vector (solid lines) (labeled in units of 10^{-15} K m^{-2} s^{-1}) at 400 hPa (lower panel) and at 250 hPa (upper panel) corresponding to the time interval from 9 May, 00 to 06 UTC. The very thick lines are the paths of columns b and d (Figure 5) during this time interval.*

400 hPa (lower panel), on 9 May 1996, between 00 UTC and 06 UTC, verifies these expectations. At 400 hPa (in the troposphere) an area with intense *vector*-frontogenesis is observed around the base of the trough with Q-vectors pointing eastwards, as expected. At 250 hPa (in the stratosphere) the opposite pattern, although slightly less intense, is observed.

A column of air between these pressure levels approaching the trough-axis from the west (see Figure 5) and entering into this area will experience a 'downward pull' at its base (due to Q-vector divergence) while it will experience an 'upward pull' at its top (due to Q-vector convergence). The consequent vortex stretching could thus serve as the explanation of the increase of the absolute vorticity along the axis of the trough (see Figure 1).

Since the 400 hPa level is located slightly below the 310 K isentropic level, while the 250 hPa level is located slightly above the 320 K isentropic level, we may consider the conditions at 400 hPa (at 250 hPa) as representative of the conditions at the base (at the top) of the columns considered in Figure 5. The trajectories of two of these columns (columns b and d), during the six-hour averaging period (between 00 UTC and 06 UTC on 9 May 1996), are shown in Figure 8. Both for trajectory 'b' as well as for trajectory 'd' the 'pull' is predominantly downward at 400 hPa and predominantly upward at 250 hPa. The absolute vorticity of column b is 22×10^{-5} s^{-1} on 9 May at 00 UTC and 27×10^{-5} s^{-1} six hours later. The absolute vorticity of column d is 19×10^{-5} s^{-1} on 9 May at 00 UTC and 23×10^{-5} s^{-1} six hours later.

Figure 9 demonstrates that the dipole pattern in the Q-vector divergence at the base of the 400 hPa trough persists for more than 12 hours and even increases in intensity with time. This is an indication of the existence of a positive feedback in which the relative vorticity increases due to vortex stretching induced by 'opposite vector-frontogenesis' while this increase in the relative vorticity, in turn, leads to an intensification of the frontogenetic effect (Equation 7). The term 'opposite vector-frontogenesis' refers to the situation in which Q-vectors point in opposite directions, respectively, above and below a specific level, which in this case is the level where the horizontal (isobaric) temperature gradient changes sign. This typically happens near or at the tropopause. It should be noted again that, following Keyser *et al*. (1988), the concept of frontogenesis here encompasses both changes in the magnitude of the temperature gradient as well as changes in the direction of the temperature gradient. Within the trough studied here the latter effect is dominant, since Q-vectors are predominantly parallel to the isotherms. As an air parcel travels through the base of the trough from west to east, the temperature gradient (a vector) across the air parcel changes direction from west to east in the troposphere and from east to west in the stratosphere.

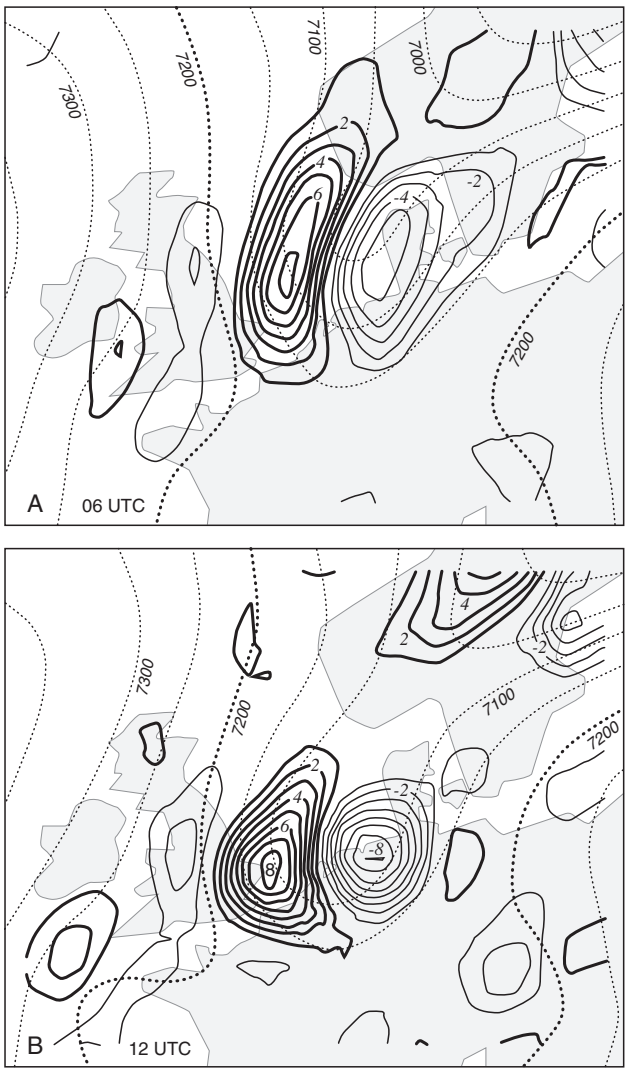

Figure 9. *Isopleths of the isobaric height (thin lines) (labeled in m) and the divergence of the Q-vector (labeled in units of 10^{-15} K m^{-2} s^{-1}) at 400 hPa corresponding to 9 May, 06 UTC (a) and 9 May, 12 UTC (b).*

According to quasi-geostrophic theory, thermal wind balance can be preserved only if the motion is downward (upward) in the troposphere (stratosphere) to the west of the trough and upward (downward) in the troposphere (stratosphere) to the east of the trough.

Unfortunately, the interpretation of the analysis of the Q-vector is questionable in the areas where the geostrophic relative vorticity is greater than the planetary vorticity, because in that case a basic assumption of quasi-geostrophic theory is violated (Holton 1992). In Figure 1 we observe that the relative vorticity is significantly greater than f in a large area near the axis of the trough. We nevertheless conclude tentatively that vortex stretching is forced by 'opposite vector-frontogenesis' in the base of a trough near the tropopause.

Although we have identified a mechanism which could serve as a partial explanation for the observed increase of the absolute vorticity (see Figure 1) prior to the formation of a cut-off low, it is obvious that the pattern

of the Q-vector divergence in the vicinity of the tropopause associated with this mechanism (see Figure 8) is by no means unique to an upper level trough which is on the verge of 'producing' a cut-off low. It is observed in nearly all upper level tropospheric troughs which are embedded in a meridional temperature gradient. Thus, we are still confronted with the following question. What causes the anomalous behaviour of the trough under investigation? The answer to this question must lie in the three-dimensional properties of the potential vorticity field.

5. Unsteady behaviour induced by events at other levels

It is well known that the dynamical effect of PV-advection at a specific level penetrates vertically over a characteristic 'distance' referred to as the Rossby height (see Hoskins *et al*. 1985: 902). In isentropic coordinates the vertical penetration 'distance' of an anomaly is

$$\Delta\theta \equiv L\sqrt{\frac{\rho\theta f\Delta Z_\theta}{g}}. \qquad (8)$$

Here, L is the horizontal scale of the potential vorticity anomaly ΔZ_θ and ρ is the density. The horizontal scale of the anomaly at 310 K is approximately 500 km (see Figure 3) and ΔZ_θ is in the order of 2 PVU, $\Delta\theta$ is in the order of 20 K. Therefore, the events at 310 K (at about 6000–7000 m) influence the PV-distribution at levels between 290 K (at about 3000 m) and 330 K (at about 10000 m). At 300 K the PV in the area in question hardly exceeds a value of 1 PVU, while PV-advection is everywhere smaller than 0.1 PVU hr^{-1}. So, events at this level are too weak to influence the flow at 310 K. At 320 K (about 9500 m) we find that there is in fact a second potential vorticity anomaly, also possessing a horizontal scale in the order of 500 km, which is advected from the west into the region of the potential vorticity anomaly under study (referred to from now on as the primary anomaly), which is also advected in an easterly direction (Figure 10). The origin

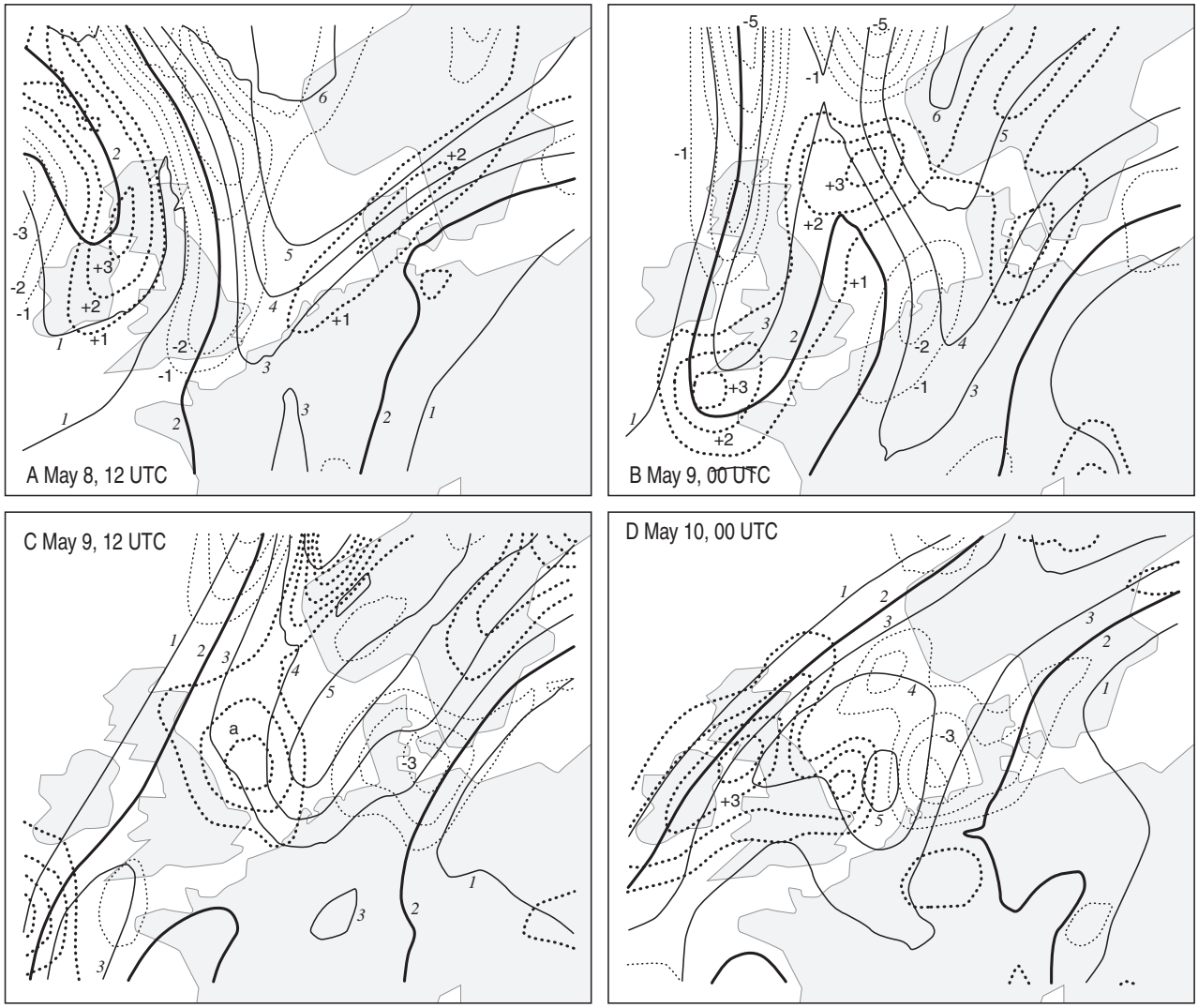

Figure 10. *Distribution of the isentropic potential vorticity (solid lines; labels in PVU; 1 PVU is 10^{-6} K m^{2}Kg^{-1}s^{-1}) and of the advection of potential vorticity (grey lines; labels in units of 0.1 PVU hr^{-1}) within the layer 315–325 K over western Europe on 8 May, 12 UTC (A); 9 May, 00 UTC (B); 9 May, 12 UTC (C); and 10 May, 00 UTC (D).*

of the second PV-anomaly on the 320 K surface, which is in fact not observed in the PV-field on the 310 K surface (see Figure 3), will not be investigated here. We are only interested in the effect that this anomaly has on the flow field at 310 K. The primary anomaly is also present at 320K. On 9 May the second anomaly merges with the primary anomaly. The flow-field at 310 K is distorted by the events at 320 K. This induces a drastic change in the distribution of the PV-advection around the primary anomaly at 310 K (Figure 3), with negative PV-advection changing into positive PV-advection in the rear of this anomaly between 00 UTC and 12 UTC on 9 May 1996 (compare Figures 3b and 3c). Obviously, this effect arrests the propagation in an easterly direction of the primary anomaly, especially near its base, where the effect is strongest.

6. Unstable isentropic downgliding and upgliding and non-adiabatic effects

In this section we investigate the importance of non-adiabatic effects and we present evidence for unstable isentropic down- and upgliding in the troposphere near the base of the trough. We first write down the potential temperature equation as follows:

$$\frac{\mathrm{d}\theta}{\mathrm{d}t} = \frac{J}{\Pi}. \tag{9}$$

Here θ is the potential temperature, J is the heating per unit mass, per unit time and Π is the Exner function ($=c_{\mathrm{p}}T/\theta$). Equation 8 can be recast into the following form (Saucier 1955):

$$\frac{\mathrm{d}\theta}{\mathrm{d}t} = \frac{\partial\theta}{\partial z}\left(w - w_{\mathrm{ad}}\right), \tag{10}$$

where

$$w_{\mathrm{ad}} \equiv \left(\frac{\partial z}{\partial t}\right)_{\theta} + u\left(\frac{\partial z}{\partial x}\right)_{\theta} + v\left(\frac{\partial z}{\partial y}\right)_{\theta} \tag{11}$$

is the 'adiabatic' vertical component of the velocity. The first term on the right-hand side of Equation 11 represents the local change in time of the height of the isentropic surface. In stationary conditions this term is equal to zero. The second and the third terms on the right-hand side of Equation 11 represent the vertical component of the advection on an isentropic surface, analogous to 'uphill' or 'downhill' motion of air parcels, because $(\partial z/\partial x)_{\theta}$ and $(\partial z/\partial y)_{\theta}$ represent the slope of the isentropic surface in the x and y directions, respectively. The heating, $\mathrm{d}\theta/\mathrm{d}t$, can be estimated from Equation 10 with the ECMWF-analysis of w and with w_{ad} estimated from Equation 11 using the ECMWF-analysis of the isentropic height and the isentropic velocity.

Figure 11 shows the result for four 6-hour intervals between 18 UTC on 8 May and 18 UTC on 9 May 1996. It appears that heating occurs principally in an area a few hundred kilometres to the east of the trough axis, where the average motion is upwards according to the ECMWF analysis. Presumably this heating is due to latent heat release. Some patches of relatively weak cooling are observed, for instance over the North Sea, a few hundred kilometres to the north of the base of the trough. The exact reason for the existence of this relatively small area of weak cooling (about 0.2 K hr^{-1}) cannot be given.

Over the southern North Sea, at the base of the trough, we observe an area of relatively intense downward motion (see Figure 11). In this area, which is the area where the cut-off low emerges during this time span, heating or cooling is negligible. Therefore, the motion in this area is approximately adiabatic. The shading in Figure 11 indicates the areas where either

$$\left(\frac{\partial z}{\partial t}\right)_{\theta} > +1 \text{ cm s}^{-1} \text{ and } w < -1 \text{ cm s}^{-1} \tag{12a}$$

or

$$\left(\frac{\partial z}{\partial t}\right)_{\theta} < -1 \text{ cm s}^{-1} \text{ and } w > +1 \text{ cm s}^{-1} \tag{12b}$$

If condition 12a is satisfied the motion is referred to as 'unstable isentropic downgliding', whereas if condition 12b is satisfied the motion is referred to as 'unstable isentropic upgliding'. The exact conditions for unstable isentropic down- or upgliding are actually

$$\left(\frac{\partial z}{\partial t}\right)_{\theta} > 0 \text{ and } w < 0$$

and

$$\left(\frac{\partial z}{\partial t}\right)_{\theta} < 0 \text{ and } w > 0,$$

respectively. But, because we are not very confident about the identification of these areas due to the low resolution in time of the analysis, we only show areas where the stronger criterium (12a or 12b) is satisfied. The existence of such areas is an indication of baroclinic instability. Incontrovertible evidence of the existence of baroclinic instability, however, should contain a consideration of an *interchange* of air parcels that are descending with neighbouring air parcels that are ascending (Green 1999), where both the ascending and the descending air parcels are moving along a path with a slope that is less than the mean slope of the isentropes, i.e. where either one of the conditions listed in (12) is satisfied. If this is the case, the kinetic energy is increasing at the expense of the available potential energy, implying baroclinic instability.

The most prominent area where one of the conditions listed in (12) is satisfied is the one with downward motion. This feature, to which we would like to assign the term 'baroclinic downburst', covers a few hundred

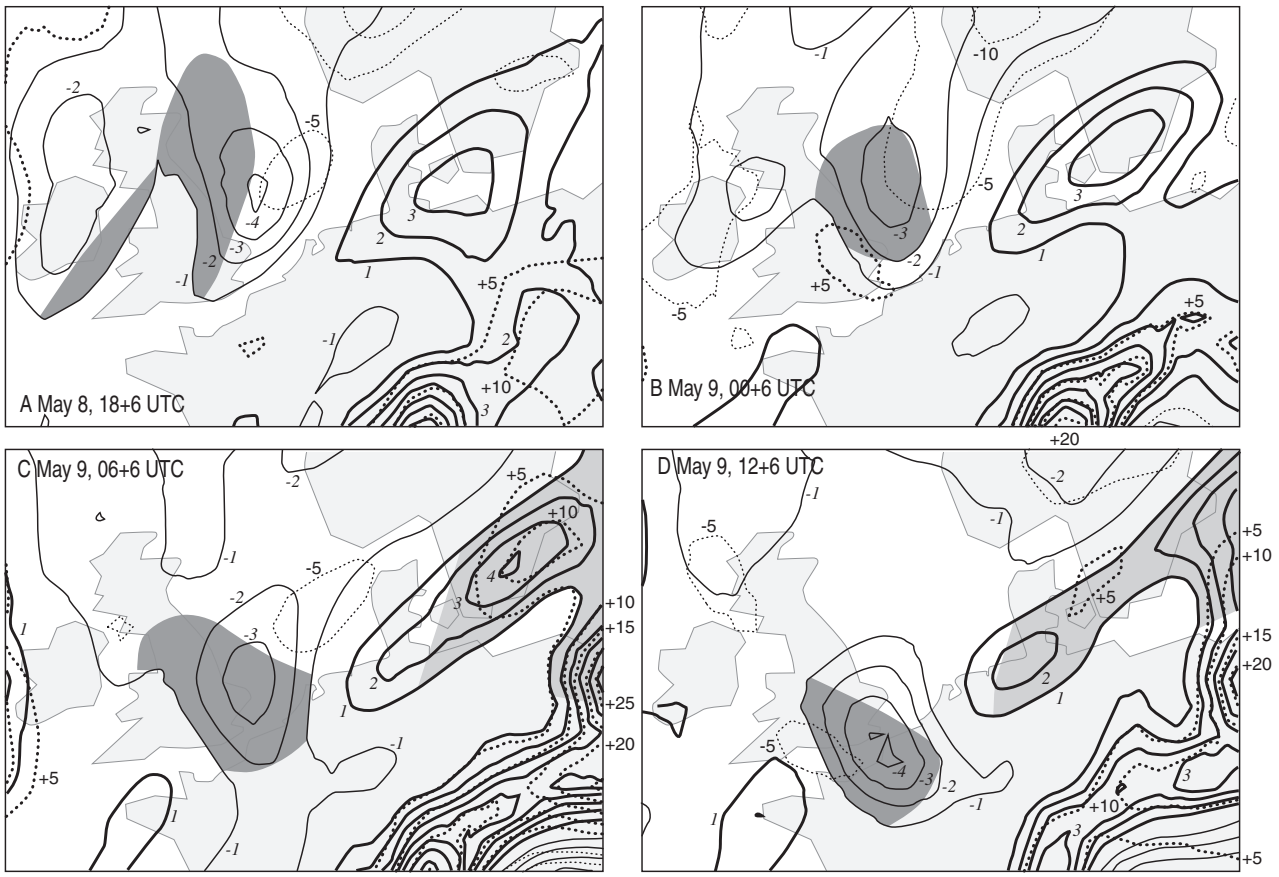

Figure 11. *Isopleths of the mean vertical velocity (according to the ECMWF-analysis) (solid lines; labeled in cm s^{-1}) and the heating rate (stippled lines; labeled in units of 10^{-5} K s^{-1}) at the 310 K isentropic level (about 7000 m) corresponding to the following consecutive time intervals: A. 8 May, 18 UTC to 9 May, 00 UTC; B. 9 May, 00 UTC to 06 UTC; C. 9 May, 06 UTC to 12 UTC; D. 9 May, 12 UTC to 18 UTC. Dark shading indicates an area where $(\partial z/\partial t)_\theta$>+1 cm s^{-1} and w<-1 cm s^{-1}), while light shading indicates an area where $(\partial z/\partial t)_\theta$<-1 cm s^{-1} and w>1 cm s^{-1}).*

thousand square kilometres. It is recognised as a coherent structure, moving slowly southwards, during a period of at least 24 hours. Not surprisingly, the location, shape and dimension of this structure bears some resemblance to the dark (dry) region seen in the corresponding water vapour image displayed in Figure 12. This area would be identified by a synoptician as a 'dry intrusion' (Browning 1997). Note should be taken (in Figure 12) of the filament of dry air joining the vortex to the trough in the north. This detail suggests that the cyclone is not in fact cut off from the stratospheric reservoir on 9 May as is suggested by the ECMWF analysis. Presumably, the cut-off is eventually effected some time after this date as the filament becomes thinner and, therefore, increasingly susceptible to some kind of 'dissipation'. The ECMWF analysis, however, is unable to resolve these features and events.

The region with unstable isentropic downgliding (the baroclinic downburst) appears first in the northerly airstream over the United Kingdom and the North Sea between 18 UTC (8 May) and 00 UTC (9 May) (Figure 11a). It seems to be 'induced' by the second anomaly observed at 320 K (see Figure 10). At the leading edge of this anomaly there is a zone of strong positive local isentropic height tendency. This zone travels into the existing zone of subsidence (at 310 K), associated with the primary anomaly. The region with unstable isentropic downgliding disappears on 10 May.

The speed of travel of the baroclinic downburst is smaller than the speed of travel of individual air parcels or air columns (compare Figure 5 with Figure 11). Therefore, air parcels travel through this region.

7. Conclusion

It is well known that a cyclone at the tropopause (a cut-off low) forms when an air mass possessing relatively high potential vorticity breaks loose from the polar source region. The invertibility principle then demands that this air mass (i.e. the cut-off low) is characterised by both high static stability and high absolute isentropic vorticity, which is indeed what is observed. However, the invertibility principle does not provide information about the actual events leading to this state. The case study described in this paper uncovers some interesting aspects of these events which are summarised in the following.

A cold core cut-off low in the upper troposphere forms within an area of unstable isentropic downgliding,

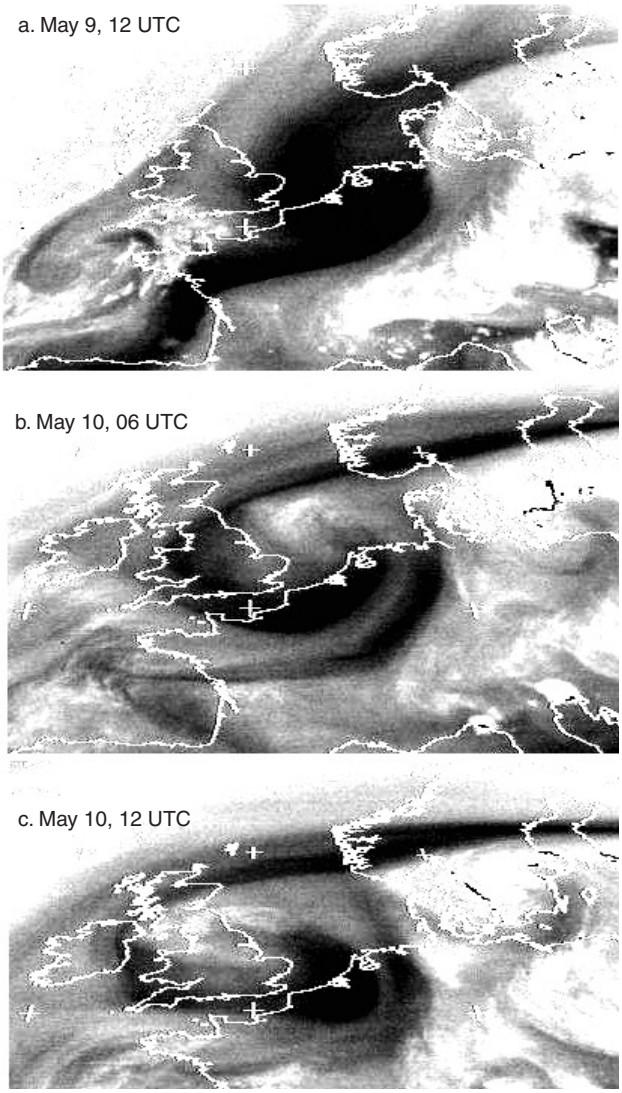

Figure 12. *Meteosat images (water vapour channel) corresponding to (a) 9 May, 12 UTC; (b) 10 May, 06 UTC; and (c) 10 May 0, 12 UTC (1996), giving the distribution of a weighted measure of the net water vapour content between 3 and 9 km height, with the largest weighting for 6–7 km (i.e. close to the 400 hPa level or the 310 K level). Dark shading indicates dry air.*

seemingly triggered by the interaction of two potential vorticity anomalies. In fact, unstable isentropic downgliding is creating the air mass possessing both relatively high static stability and relatively high absolute isentropic vorticity. The core of the cut-off cyclone forms between two vertically diverging isentropes (Figure 13). In the specific case investigated here, the 320 K surface slopes upwards towards the south, while the 310 K surface slopes downwards towards the south. An air column between these two isentropes, moving southward on the western side of a trough, will find itself in an environment with lower static stability, as is shown schematically in Figure 13. Unless stretching occurs, and a concomitant increase in vorticity, the air column will not be in 'balance' with the environment (according to the invertibility principle). In the case studied here the stretching does indeed occur and is in fact

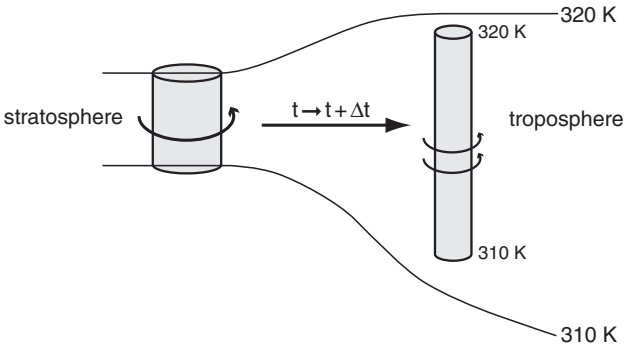

Figure 13. *Schematic picture of the events in a meridional vertical section leading to the formation of an isolated air mass with relatively high static stability and relatively high absolute vorticity. The 'environment' of the air column is represented by the two isentropes. See the text for further explanation.*

forced by 'vector-frontogenesis', working in opposite directions, respectively, at the base and at the top of the air column. This so-called 'opposite vector-frontogenesis' is confirmed by the analysis of the pattern of Q-vectors and the associated vertical motion. It must be stressed that, according to quasi-geostrophic theory, the vertical motion is the result of the material distortion of isotherms within the trough base, and the accompanying material turning of the thermal wind.

One remaining question is the following. Are the events described in this paper characteristic for other cases of tropopause cyclogenesis? An indication of an affirmative answer to this question was obtained by investigating another case of tropopause cyclogenesis, which occurred over the same area of western Europe on 16 February 2001. All the characteristic events occurring on 9 May 1996, such as the strong increase of the absolute vorticity at 400 hPa, as a response to intense Q-vector divergence on the western side of the base of the trough, coinciding with unstable isentropic downgliding, were also diagnosed in this case.

We have identified several novel synoptic features (the 'baroclinic downburst') and processes ('opposite vector-frontogenesis') that appear to play a role in tropopause cyclogenesis. Based on the case studied in this paper, our hypothesis is that the feedback between opposite vector-frontogenesis in the vicinity of the trough axis and vortex stretching is intensified for a short period of time (about 24 hours) in a restricted area (several hundred thousand square kilometres), such that there is a conversion of available potential energy into kinetic energy, as happens in baroclinic instability. Progress in the understanding of the connection between these features and their exact relation to tropopause cyclogenesis will require analyses with a much higher resolution.

Acknowledgements

We thank Jaco Bergenhenegouwen for drawing most of the figures, Jos Lelieveld for drawing our attention to relevant literature, and the reviewers for very constructive criticism.

References

Appenzeller, C., Davies, H. C. & Norton, W. A. (1996) Fragmentation of stratospheric intrusions. *J. Geophys. Res.*, 101D, 1435–1456.

Bell, G. D. & Bosart, L. F. (1993) A case study diagnosis of the formation of an upper-level cut-off cyclonic circulation over the eastern United States. *Mon. Wea. Rev.* **121**: 1635–1655.

Bell, G. D. & Keyser, D. (1993) Shear and curvature vorticity and potential vorticity interchanges: Interpretation and application to a cut-off cyclone event. *Mon. Wea. Rev.* **121**: 76–102.

Browning, K. A. (1997) The dry intrusion perspective of extra-tropical cyclone development. *Meteorol. Appl.* **4**: 317–324.

Cox, B. D., Bitchell, M. & Gray, L. J. (1997) Modelling of stratospheric intrusions within a mid-latitude synoptic-scale disturbance. *Q. J. R. Meteorol. Soc.* **123**: 1377–1403.

Edouard, S., Vautard, R. & Brunet, G. (1997) On the maintenance of potential vorticity in isentropic coordinates. *Q. J. R. Meteorol. Soc.* **123**: 2069–2094.

Eliassen, A. & Kleinschmidt, E. (1957) Dynamic meteorology. In: S.Flügge & J. Bartels (eds.), *Encyclopedia of Physics*, vol 58, pp. 1–154.

Green, J. (1999) *Atmospheric Dynamics*. Cambridge University Press. 213 pp.

Hirschberg, P. A. & Fritsch, J. M. (1991a) Tropopause undulations and the development of extratropical cyclones. Part I: Overview and Observations from a Cyclone Event. *Mon. Wea. Rev.* **119**: 496–517.

Hirschberg, P. A. & Fritsch, J. M. (1991b) Tropopause undulations and the development of extratropical cyclones. Part II: Diagnostic analysis and conceptual model. *Mon. Wea. Rev.* **119**: 518–553.

Holopainen, E. O. & Rontu, L. (1981) On shear lines in the upper troposphere over Europe. *Tellus* **33**: 351–359.

Holton, J. R. (1992) *An Introduction to Dynamic Meteorology*, third edition. Academic Press. 507 pp.

Hoskins, B. J. (1991) Towards a *PV-q* view of the general circulation. *Tellus* **43AB**: 27–35.

Hoskins, B. J. (1997) A potential vorticity view of synoptic development. *Meteorol. Appl.* **4**: 325–334.

Hoskins, B.J., McIntyre, M. E. & Robertson, A. W. (1985) On the use and significance of isentropic potential vorticity maps. *Q. J. R. Meteorol. Soc.* **111**: 877–946.

Hsieh, Y.P. (1949) An investigation of a selected cold vortex over North America. *J. Meteorol.* **6**: 401–410.

Hsieh, Y-P. (1950) On the formation of shear lines in the upper atmosphere. *J. Meteorol.* **7**: 382–387.

Keyser, D., Reeder, M. J. & Reed, R. J. (1988) A generalization of Pettersen's frontogenesis function and its relation to the forcing of vertical motion. *Mon. Wea. Rev.* **116**: 762–780.

Kleinschmidt, E. (1950a) Uber aufbau und entstehung von zyklonen. I. Teil. *Meteor. Rundschau.* **3**: 1–7.

Kleinschmidt, E. (1950b) Uber aufbau und entstehung von zyklonen. II. Teil. *Meteor. Rundschau*. **3**, 54–61.

Kurz, M. (1997) The role of frontogenetic and frontolytic wind field effects during cyclone development. *Meteorol. Appl.* **4**: 353–363.

Mesinger, F. & Arakawa, A. (1976) *Numerical Methods used in Atmospheric Models.* Garp Publications Series, no.17.

Newton, C. W., Phillips, N. A., Carson J. E. & Bradbury, D. L. (1951) Structure of shear lines near the tropopause in summer. *Tellus* **3**: 154–171.

Palmen, E. (1949) On the origin and structure of high-level cyclones south of the maximum westerlies. *Tellus* **1**: 22–31.

Palmen, E. & Newton, C. W. (1969) *Atmospheric Circulation Systems*. Academic Press, 603 pp.

Polvani, L. M. & Plumb, R. A. (1992) Rossby wave breaking, microbreaking, filamentation, and secondary vortex formation: The dynamics of a perturbed vortex. *J. Atmos. Sci.* **49**: 462–476.

Saucier, W. J. (1955) *Principles of Meteorological Analysis*. University of Chicago Press, 438 pp.

Thorncroft, C. D., Hoskins, B. J. & McIntyre, M. E. (1993) Two paradigms of baroclinic-wave life-cycle behaviour. *Q. J. R. Meteorol. Soc.* **119**: 17–55.

Thorpe, A. J. (1985) Diagnosis of balanced vortex structure using potential vorticity. *J. Atmos. Sci.* **42**: 397–406.